Journal of Geochemical Exploration 176 (2017) 136–145

Contents lists available at ScienceDirect

Journal of Geochemical Exploration

journal homepage: www.elsevier.com/locate/jgeoexp

High-resolution enrichment of trace metals in a west coastal wetland of the southern Yellow Sea over the last 150 years

Kunshan Bao [a,*], Ji Shen [a], Atindra Sapkota [b]

[a] State Key Laboratory of Lake Science and Environment, Nanjing Institute of Geography and Limnology, Chinese Academy of Sciences, Nanjing 210008, China
[b] State Key Laboratory of Environmental Geochemistry, Institute of Geochemistry, Chinese Academy of Sciences, Guanshui Road 46, Guizhou 550002, China

ARTICLE INFO

Article history:
Received 4 March 2015
Revised 24 July 2015
Accepted 16 September 2015
Available online 24 September 2015

Keywords:
Coastal wetlands
Trace elements
Environmental pollution
Historical trends
^{210}Pb-dating
China

ABSTRACT

The objectives of this study were to determine the concentrations and accumulation rates of trace metals in the Yancheng coastal wetland of Jiangsu province, China, and to assess their relationship to establish a history of anthropogenic metal emissions. To address these aims, we analyzed 26 major and trace elements using ICP-AES and ICP-MS in two sediment sections dated by ^{210}Pb and ^{137}Cs techniques (approximately spanning the last 150 years). Physicochemical parameters including bulk density, water content, mass magnetic susceptibility and grain-size composition were also documented. The relationship between these factors was examined through a correlation analysis, and two principal components were discriminated by a principal component analysis (PCA) based on eigen-values > 1 and explaining 85% of the total variance of the element concentrations: the first component covering As, Cd, Pb, Sb and Zn is associated with an anthropogenic source, and the second component representing Al, Cu, K, Rb, and Sr reflects a lithogenic source. The first group also includes Fe and Mn and probably reflects the influence of the redox status during the geochemical process. The accumulation rates and enrichment factors of the trace metals suggest an increasing pollution pattern, especially for the last 20 years. The reconstructed history of trace metal pollution over the past 150 years is consistent with the industrial development in Jiangsu province and clearly illustrates the influence of human activities on the local environment. This high resolution geochemical dataset for the Yancheng coastal wetland is helpful for understanding the deposition processes and reconstructing the past pollution history from anthropogenic activities in the area.

1. Introduction

Trace metals have been emitted by human activities and dispersed into the environment since the beginning of metallurgy (Nriagu, 1996). They usually have many adverse impacts on environmental and human health because of their toxic, persistent and bio-accumulative nature. In addition to natural sources, including volcanic activity, soil erosion and biologically driven reduction processes in the ocean, anthropogenic sources are the major contributors to the abundance of trace metals in the environment and principally include fossil-fuel combustion; industrial manufacturing; ore mining and processing; and the incineration of urban, medical and industrial wastes (Pacyna and Pacyna, 2001). Human activities have been shown to increase local, regional and global fluxes of trace metals to the atmosphere, and anthropogenic trace metal fluxes clearly exceed prehistoric levels of atmospheric deposition. As a result, governments worldwide have negotiated a global legally binding instrument to control trace metal emissions from human activities, such as the substantiation documents for the United Nations (UN)/Economic Commission for Europe (ECE) protocol on the emission reductions of trace metals (UNECE, 1994).

A considerable percentage of trace metals released to the atmosphere is often carried by long-range transport, deposited by precipitation or as aerosols and stored in and between aquatic and terrestrial ecosystems in remote areas. Long-term records to quantify the accumulation of trace metals in natural geological archives are helpful to differentiate and document the temporal trends of natural versus anthropogenic trace metals (Le Roux et al., 2004; Bindler et al., 2012). The magnitude and history of changes in past metal deposition have been studied in a variety of environmental records in the northern hemisphere, such as ice cores (Hong et al., 1994), lake sediments (Rydberg and Martinez Cortizas, 2014) and wetland sediments (Martinez Cortizas et al., 2013; C. Gao et al., 2014). The investigations above have focused on geochemical analyses of sediments sampled at different depths and the establishment of rates of sediment accumulation through ^{14}C or ^{210}Pb dating to provide information about the pollution chronologies. The fluxes in atmospheric trace metal deposition can be calculated by combining the rate of sediment accumulation, dry bulk density and trace metal concentrations.

* Corresponding author.
E-mail address: ksbao@niglas.ac.cn (K. Bao).

http://dx.doi.org/10.1016/j.gexplo.2015.09.010
0375-6742/

Coastal wetlands are ecosystems which exist within an elevation gradient ranging between the landward edge where the sea passes its hydrologic influence to groundwater and atmospheric processes and the subtidal depths to which light penetrates to support the photosynthesis of benthic plants (Perillo et al., 2009). They are complex and diverse, including salt marshes, mangroves, tidal flats and sea grasses, and thus rank among the most productive of all natural ecosystems (Leorri et al., 2013). As one of the most significant ecosystems in the world, coastal wetlands have many intrinsic values, including high resilience against extreme weather, wide varieties of plant and animal species and significant socioeconomic benefits to fisheries (Pennings, 2012). Coastal wetland regions have been attractive sites for human settlement over several millennia, and continued population growth and increasing global food demand has led to the conversion of approximately 25–50% of the world's coastal wetlands into farmland and aquafarms (Regnier et al., 2013). In addition, anthropogenic contamination has been increasing, particularly due to land use changes, the discharge of sewage from urban areas and industrial emissions over the past decades (Monteiro et al., 2012). Among the pollutants released to coastal environments by human activities, heavy metals are the most persistent, and they have received extensive attention over the world (Jayaprakash et al., 2010; Mahiques et al., 2013).

In China, meeting future food and energy demands while mitigating the potential detrimental environmental impacts has emerged as one of the greatest challenges in the exploitation and conservation of coastal wetlands (Kirwan and Megonigal, 2013). For example, the tidal flats in north Jiangsu province are the largest coastal wetlands in China and world-renowned habitats for many rare and endangered species. Although two wetland reserves of international importance, the Dafeng National Nature Reserve (Ramsar site no. 1145) and the Yancheng National Nature Reserve (YNNR, no. 1156), have been established, the outlook for protection is not optimistic (Bao, 2015). From 1988 to 2006, the decrease in grass flats in the YNNR was ca. 900 ha yr^{-1}, but the increase in farmland and pond areas was ca. 600 ha yr^{-1} and 1400 ha yr^{-1}, respectively (Ke et al., 2011). This is not an individual case in China. Reportedly, 57% of China's coastal wetlands have disappeared due to land reclamation since the 1950s (Qiu, 2011).

Therefore, we analyzed multi-elements using ICP-AES and ICP-MS in two sediment cores from the Yancheng coastal wetland of northern Jiangsu, China. The objectives of this study were to determine the concentration and historical deposition of trace metals over the past 150 years using ^{210}Pb and ^{137}Cs techniques and to assess their relationship to establish a history of atmospheric metal emissions from anthropogenic sources using multivariate statistical techniques. This study is helpful for exploring the anthropogenic effects on a regional environment and providing support for policy-making in sustainable development.

2. Materials and methods

2.1. Study area

The coastal region in Yancheng, Jiangsu province, faces the Yellow Sea to the east and the Yangtze River to the south. The Yancheng wetlands cover a total area of 5.1×10^5 ha (ca. 30% of the municipality's total area) and stretch for approximately 580 km along the coast, accounting for 70% of the provincial total and 14.3% of the national total. They consist primarily of extensive inter-tidal mudflats, tidal creeks, river channels, salt marshes, reed beds and marshy grasslands that provide desirable habitats for numerous species of flora and fauna of global and national importance. Moreover, the wetlands provide important ecosystem services to local communities and also improve water quality by assimilating some of the household and industrial wastes that are rapidly increasing in Yancheng municipality. The Yancheng wetlands have become a hotspot of wetland research for their significance and were listed in the world network of biosphere conservation (WNBP) by the United Nations in 1992. However, the natural wetlands along the Yancheng coast have been experiencing rapid degradation due to rapid economic development as well as frequent land use changes (Ke et al., 2011; Chuai et al., 2014). Anthropogenic land uses along this coastal region include mainly agriculture, aquaculture and solar salt production. In recent times, the human activities of harbor building, wind power generation and tourism have increased. The associated sewage and solid wastes are also increasing (Chuai et al., 2014).

The sampling site is situated in Sheyanggang, Yancheng (Fig. 1), which is a typical tidal ecosystem and very close to Xingyanggang in the same region. At present, the wetland landscape from sea to land include the following ecological zones: bare silt-sand mixed flat, *Spartina alterniflora* flat, *Suaeda salsa* flat and *Phragmites australis* flat (Gao et al., 2012). This wetland is located in the north subtropical zone with an average precipitation of 1010 mm yr^{-1} and annual average temperature of 14.4 °C. The tidal flat is affected by the marine monsoon climate with a prevailing southeastern wind in summer and a prevailing northwestern wind controlled by tropical depression in winter (Liu et al., 2010). This site is a plain sedimentary geomorphology (average slope: 0.055%) formed by the river fluvial and coastal sediment processes since the end of the late Pleistocene. The average tidal range is 3.68 m. The soils could be classified into Anthrosols, Fluvisols and Cambisols according to the formation process (Fang et al., 2010).

2.2. Core-sampling and slice-sectioning

Two sediment cores were collected using a gasoline-motorized corer (Eijkelkamp, Netherlands) from the *S. alterniflora* flat (labeled SAF-1, N 33°46′34″, E 120°31′49″, Altitude 3 m) and the bare flat (labeled BAF-1, N 33°44′37″, E 120°31′50″, Altitude 1 m) in October 2013. The latitude, longitude and altitude at the sampling sites were determined with a portable global positioning system (Garmin GPS 62SC, Garmin International, Olathe, KS). Back at the laboratory, the core was split, with one half archived in frozen condition and the other half was precisely cut into 1 cm slices using a stainless steel semicircle blade of a half pipe-diameter size. All slices were packed into labeled zip-lock polyethylene plastic bags for storage and further preparation.

2.3. Physical and chemical analysis

The water content (%) and dry bulk density (g cm^{-3}) of the samples were determined by weighing a volumetric sub-sample of each slice of the sediment cores before and after freeze drying overnight. The mass magnetic susceptibility was quantified from the homogenized, dried samples using a Bartington Instruments MS2 sensor. The particle size spectra were determined using a Malvern automated laser-optical particle-size analyzer (Mastersizer-2000; Malvern Instruments Ltd, Worcestershire, U.K.) after the removal of organic matter by 10% hydrogen peroxide (H_2O_2) and of carbonate by 10% hydrochloric acid (HCl). This instrument has a measurement range of 0.02 to 2000 μm and an accuracy of less than 3% with repeated measurement error.

2.4. Determination of age using ^{210}Pb and ^{137}Cs

The bulk-weighed, dry samples were sealed in plastic test tubes with caps for ^{210}Pb dating by gamma spectrometry with well-type coaxial low background intrinsic germanium detectors (Ortec HP Ge GWL series, Oak Ridge, TN, U.S.A.). The radioactivity levels of ^{210}Pb were determined via gamma emissions at 46.5 keV. The emissions of ^{226}Ra with the 295 keV and 352 keV γ-rays emitted by its daughter nuclide ^{214}Pb were determined after 3 weeks of storage in sealed containers to allow for radioactive equilibrium. The radioactivity of ^{137}Cs was measured with the 662 keV photo peak. The standard sources and sediment samples of known activity were provided by the China Institute of Atomic Energy and used to calibrate the absolute efficiencies of the detectors. The counting times of ^{137}Cs and ^{210}Pb were typically in the

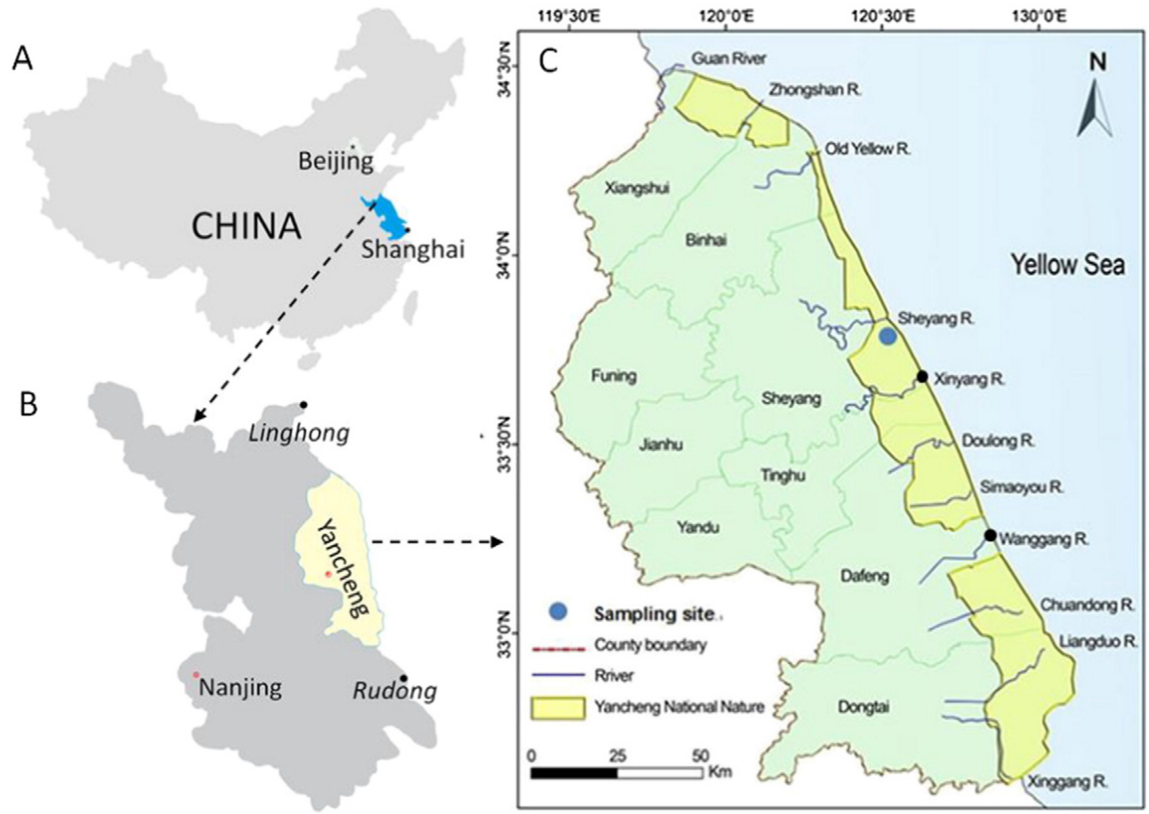

Fig. 1. (A) Map of China showing the location of Jiangsu province. (B) Map of Jiangsu province showing location of Yancheng city. (C) Map of Yancheng showing the National Nature Reserve area and the sampling site. Xingyang wetland (Liu et al., 2010), Wanggang wetland (Wang et al., 2005), Linghong wetland (Liu et al., 2013) and Rudong wetland (Zhang et al., 2014) in Jiangsu province for comparison in Table 2 are also shown.

range of 50,000 to 86,000 s, providing a measurement precision of between ±5% and ±10% at the 95% level of confidence, respectively. The supported ^{210}Pb in each sample was assumed to be in equilibrium with the in-situ ^{226}Ra, and unsupported ^{210}Pb activities were determined from the difference between the total ^{210}Pb and the supported ^{210}Pb activity.

2.5. Analysis of major and trace elements

Twenty-six elements (Al, As, Ba, Be, Ca, Co, Cr, Cu, Cd, Cs, Fe, K, Li, Mg, Mn, Mo, Na, Ni, Pb, Rb, Sr, Sb, Ti, Tl, V and Zn) were measured with an Atomic Emission Spectroscopy with Inductively Coupled Plasma (ICP-AES Prodigy 7, Teledune Leeman Labs, USA) and a Quadrupole Inductively Coupled Plasma Mass Spectrometry (Q-ICP-MS 7700x, Agilent Technologies, USA). The digestion procedure for the elemental analyses is as follows. Sample aliquots were dried at 105 °C for 12 h and ground using an agate mortar. The fine sample was weighed accurately (0.2000–0.2059 g) into a TFM-PTFE in-liner vessel ("bomb") with the stainless steel pressure digestion system (DAB-2, Berghof, Germany). Next, 2.5 mL HNO_3 (high purity obtained by the sub-boiling distillation of the analytical-grade reagent in an I.R. distiller (BSB-939, Berghof, Germany)) and 0.5 mL H_2O_2 (Baker ACS Reagent) were added, and the PTFE vessels were close heated at 200–220 for 3 h. After cooling, 1 mL HF (Baker ACS Reagent) and 0.5 mL $HClO_4$ (Fisher Trace Metal Grade) were added, and they were heated again until the white smoke from the in-liner disappeared. After cooling again, 0.5 mL HNO_3 (high purity) and little deionized water (>18 MΩ cm) were added, and they were heated at 150–180 for 5 min. Lastly, they were cooled to ambient temperature for a minimum of 2 h, and the digested samples were transferred to a 50 mL centrifuge tube along with the washings from the TFM-PTFE in-liner. The sample solutions were brought up to a final volume of 25 mL with deionized water for the trace metal analysis. For quality control, a reference standard consisting of stream sediments (GBW07358, Institute of Geophysical and Geochemical Exploration, Langfang, China) was used during the elemental measurement process. The average measured concentrations of all of the measured elements for the reference materials and their respective values measured independently by the Institute of Geophysical and Geochemical Exploration are given in Table 1. The limit of detection (LOD) is given as three times the relative standard deviation (RSD) of three blind replicates. The triplicate measurements of the standards show a precision better than 8% except for Sb, which presents a precision of 17%. The accuracies range from −7% to 9% for most of the elements except for As (12%), Ni (16%) and Sb (16%).

2.6. Calculations of flux and enrichment factors

The core chronology was determined using the unsupported ^{210}Pb and ^{137}Cs with the application of the constant rate of supply (CRS) model due to tidal and anthropogenic effects, resulting in varying sedimentary rates (Appleby, 2008). The equations for the ^{210}Pb-inferred chronologies and sediment rate (cm yr^{-1}) have been provided in detail elsewhere (Bao et al., 2010). To estimate the inventories and burial fluxes of the sediment mass and the trace metals in the sediment cores of a given area, several sediment properties including dry bulk density, sediment rate and sediments porosity (dimensionless) must be considered in addition to the sediment mass and trace metal concentration. The sediment porosity was defined as one minus the ratio of the dry bulk density and the solid-grain density, which was 2.7 g cm^{-3} (Baldwin and Butler, 1985) according to Eq. (1). The mass accumulation rate (g cm^{-2} yr^{-1}) and the accumulation rates of the trace metals (mg m^{-2} yr^{-1}) were estimated by Eqs. (2) and (3). A common approach for distinguishing between natural and anthropogenic sources for elements in the environment is to calculate a normalized

Table 1
Statistical summary of mean, maximum (Max) and minimum (Min) concentrations of elements of the two investigated sediment core samples from Yancheng coastal wetland in Jiangsu province, China.

Element	SAF-1 core (n = 28)				BAF-1 core (n = 20)				Reference measured[a]			Certified value	LOD[b]
	Min	Max	Mean	$Factor_{max/min}$	Min	Max	Mean	$Factor_{max/min}$	Min	Max	Mean (n = 3)		
Al ($mg\ g^{-1}$)	51.40	73.40	63.69	1.43	49.00	65.63	55.87	1.34	57.50	58.10	57.73 ± 0.32	58.54 ± 0.69	0.01
As ($mg\ kg^{-1}$)	9.15	27.33	15.32	2.99	9.40	15.83	11.44	1.68	15.00	16.70	16.00 ± 0.88	14.3 ± 0.9	0.1
Ba ($mg\ kg^{-1}$)	389.67	436.67	406.94	1.12	391.67	436.33	417.65	1.11	453.00	455.00	453.67 ± 1.15	455 ± 9	0.5
Be ($mg\ kg^{-1}$)	1.50	2.73	2.01	1.82	1.07	2.07	1.62	1.93	2.20	2.30	2.23 ± 0.06	2.2 ± 0.1	0.05
Ca ($mg\ g^{-1}$)	37.35	49.72	43.94	1.33	35.60	58.03	39.76	1.63	21.10	21.20	21.17 ± 0.06	21.16 ± 0.28	0.005
Co ($mg\ kg^{-1}$)	7.70	17.17	12.684	2.23	7.83	13.67	9.68	1.75	10.20	10.40	10.27 ± 0.12	10.2 ± 0.4	0.01
Cr ($mg\ kg^{-1}$)	53.00	92.00	76.884	1.74	44.33	78.67	59.57	1.77	66.00	67.00	66.33 ± 0.57	61 ± 4	1.5
Cu ($mg\ kg^{-1}$)	11.95	47.00	25.38	3.93	10.43	27.07	16.09	2.60	132.00	144.00	139.00 ± 6.24	132 ± 5	0.02
Cd ($mg\ kg^{-1}$)	0.09	0.23	0.16	2.56	0.09	0.15	0.11	1.67	0.34	0.38	0.36 ± 0.02	0.34 ± 0.02	0.01
Cs ($mg\ kg^{-1}$)	4.15	11.40	8.23	2.75	3.20	8.93	5.55	2.79	5.70	5.80	5.77 ± 0.06	5.8 ± 0.3	0.01
Fe ($mg\ g^{-1}$)	23.00	40.40	32.37	1.76	21.90	33.37	25.67	1.52	46.10	47.20	46.50 ± 0.61	48.96 ± 0.70	0.002
K ($mg\ g^{-1}$)	16.40	22.77	19.91	1.39	15.33	20.73	17.85	1.35	19.50	19.60	19.53 ± 0.06	19.51 ± 0.25	0.03
Li ($mg\ kg^{-1}$)	22.80	56.87	41.62	2.49	20.03	43.03	29.04	2.15	21.00	22.00	21.33 ± 0.57	20.7 ± 2.0	0.5
Mg ($mg\ g^{-1}$)	10.10	17.43	14.22	1.73	9.67	14.67	11.34	1.52	10.10	10.10	10.10 ± 0	10.25 ± 0.18	0.002
Mn ($mg\ kg^{-1}$)	457.00	1052.33	732.68	2.30	425.67	693.00	514.70	1.63	1396.00	1416.00	1407.30 ± 10.26	1420 ± 40	0.5
Mo ($mg\ kg^{-1}$)	0.44	0.94	0.69	2.14	0.41	0.72	0.53	1.76	.95	1.07	1.02 ± 0.06	0.94 ± 0.04	0.05
Na ($mg\ g^{-1}$)	12.80	17.50	15.26	1.37	14.43	17.62	16.79	1.22	10.20	10.40	10.30 ± 0.10	10.39 ± 0.15	0.01
Ni ($mg\ kg^{-1}$)	20.67	39.33	30.92	1.90	22.67	54.67	29.80	2.41	20.00	23.00	22.00 ± 1.73	18.9 ± 0.7	2
Pb ($mg\ kg^{-1}$)	15.47	29.40	22.79	1.90	14.97	22.57	17.18	1.51	208.00	213.00	211.00 ± 2.64	210 ± 6	0.02
Rb ($mg\ kg^{-1}$)	85.75	144.00	118.17	1.68	76.97	130.67	100.69	1.70	97.00	110.00	105.00 ± 7.00	96 ± 4	0.02
Sr ($mg\ kg^{-1}$)	163.33	198.67	179.57	1.22	185.00	261.33	198.02	1.41	170.00	171.00	170.67 ± 0.58	171 ± 5	0.2
Sb ($mg\ kg^{-1}$)	1.10	1.45	1.32	1.32	1.02	1.53	1.17	1.50	1.10	1.52	1.37 ± 0.23	1.18 ± 0.07	0.05
Ti ($mg\ g^{-1}$)	3.73	4.58	4.05	1.23	3.34	5.32	3.83	1.59	3.19	3.22	3.21 ± 0.02	3.2 ± 0.1	0.001
Tl ($mg\ kg^{-1}$)	0.39	0.60	0.51	1.54	0.36	0.58	0.46	1.61	0.82	0.93	0.86 ± 0.06	0.91 ± 0.07	0.02
V ($mg\ kg^{-1}$)	63.50	101.67	84.26	1.60	58.67	86.00	68.04	1.47	77.00	80.00	78.67 ± 1.52	77 ± 3	1
Zn ($mg\ kg^{-1}$)	38.00	89.67	66.62	2.36	20.33	61.67	34.29	3.03	193.00	200.00	195.33 ± 4.04	209 ± 6	1

[a] The reference material is stream sediments (GBW07358) provided by the Institute of Geophysical and Geochemical Exploration in Langfang of China.
[b] LOD is the limit of detection defined as three times of the relative standard deviation.

enrichment factor for the metal concentrations above uncontaminated background levels (Fernandes et al., 2011; Bai et al., 2014). The calculation of the enrichment factor is usually based on a conservative (lithogenic) element indicative of mineral matter, such as Al; in addition to the reference element, such a calculation is often relative to a reference material, either external (i.e., the Earth's Upper Continental Crust (UCC)) or internal (i.e., the mean of several low-concentration samples selected from the deeper, pre-industrial levels of cores) (Eq. (4)). The interpretation of the enrichment factor is that an element with an enrichment factor value near unity has a probable source in the crustal material and elements with enrichment factor value a few to many times larger than unity could be mainly of industrial origin (Reimann and de Caritat, 2005).

$$SP = 1 - DBD/SGD \tag{1}$$

$$MAR\left(g\,cm^{-2}yr^{-1}\right) = DBD\left(g\,cm^{-3}\right) \times SR\left(cm\ yr^{-1}\right) \times (1-SP) \tag{2}$$

$$\begin{aligned} TM\,AR\left(mg\,m^{-2}yr^{-1}\right) = {} & TM\left(mg\,kg^{-1}\right) \times DBD\left(g\,cm^{-3}\right) \\ & \times SR\left(cm\,yr^{-1}\right) \times (1-SP) \times 10 \end{aligned} \tag{3}$$

$$TM\,EF = (TM/Al)_{sample}/(TM/Al)_{UCC} \tag{4}$$

where *SP* is the sediment porosity, *DBD* is the dry bulk density, *SGD* is the solid-grain density (2.7 g cm^{-3}), *MAR* is the mass accumulation rate, *SR* is the sediment rate, *TM* is the trace metal, *TM AR* is the accumulation rate of the trace metal, and *TM EF* is the enrichment factor of the trace metal. The number, 10 in Eq. (3) is a unit conversion factor.

2.7. Data statistical analysis

When a large geochemical dataset is generated in such a multi-tracer study, a principal component analysis (PCA) is often applied to reduce the number of observed variables to a smaller number of factors and to identify the sources and processes related to the distribution of multiple elements (Bai et al., 2011; Jamshidi-Zanjani and Saeedi, 2013). This statistical technique is used for a single set of variables (i.e., geochemical elements) to discern which set of variables form coherent subsets that are relatively independent of one another. Those correlated variables are combined into factors which should be representative of the underlying process. The loadings measure the correlations among these variables and relate to the specific association between the factors and original variables. The mean, standard deviation, minimum and maximum values were calculated for the variables in the cores. Correlation and PCA analyses were performed to examine the relationships among the individual parameters with a statistical significance determined at the P = 0.05 level except if indicated differently. Before the analyses, all data were converted to Z-scores calculated as in Eq. (5). These procedures were performed using SPSS 11.5 software package (SPSS, 2002).

$$Z_{-score} = (X_i - X_{avg})/X_{std} \tag{5}$$

where X_i, X_{avg}, and X_{std} are the given value, the average and the standard deviation of a variable in a given sample, respectively.

3. Results and discussion

3.1. Physicochemical properties of the sediment

The profile variations of the main grain-size fractions (clay: <2 μm, silt: 2–64 μm, and sand: >64 μm) with depth are shown in Fig. 2. The clay ranges from 5.43 to 33.39% with an average of 16.33% for SAF-1 and from 8.42 to 19.15% with an average of 12.83% for BAF-1; the silt ranges from 60.76 to 82.20% with an average of 73.05% for SAF-1 and from 56.77% to 78.72% with an average of 70.66% for BAF-1; the sand ranges from 1.17 to 27.87% with an average of 10.62% for SAF-1 and from 8.62 to 25.69% with an average of 16.51% for BAF-1. They fluctuate within a certain range in the two profiles, and the grain-size distribution is assembled with the silt fine-grain fractions over the entire core length. This is consistent with previous conclusions that the Yancheng

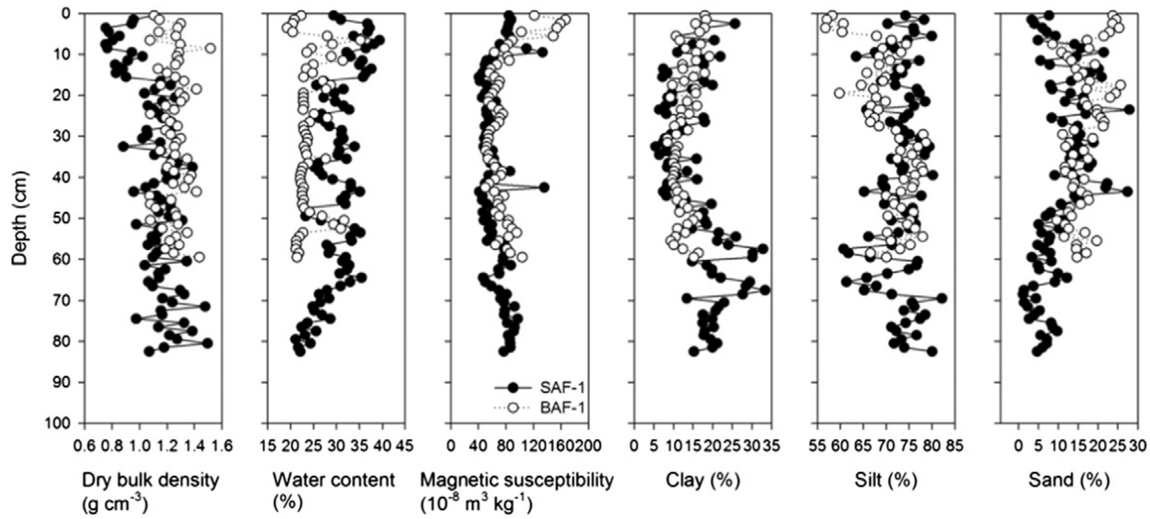

Fig. 2. Depth variations of some physical and chemical parameters of the two investigated sediment core samples from the Yancheng coastal wetland in Jiangsu province, China.

coastal wetland is a silt- to fine sand and mud-sand mixed tidal flat (Liu et al., 2010; Li and Gao, 2013). The amount of coarse particles in the SAF-1 core (a vegetated flat site) is less than in the BAF-1 core (a bare flat site) (Fig. 2), which could possibly be explained by the trapping effect of the plant obstruction to the tidal flow (Liu et al., 2013; S. Gao et al., 2014). In addition, the contribution of the decomposition of the plant residuals to the fine particles in the sediment should also be considered.

The dry bulk density ranges from 0.75 to 1.45 g cm^{-3} (SAF-1) and from 1.07 to 1.52 g cm^{-3} (BAF-1). The dry bulk density of SAF-1 increased with downward depth (Fig. 2). The pattern of both cores below ca. 20 cm is consistent. The lower values of SAF-1 versus BAF-1 for the topmost sections were likely a result of the existence of plant matter in SAF-1, where the black sediment contained a large amount of decayed *S. alterniflora*. The water content of both the SAF-1 and BAF-1 cores ranged from 20% to 40%. The distributions are similar for the two cores and characterized by the highest value occurring at the subsurface sections, with a general decrease upon moving to the deeper layers (Fig. 2). This is consistent with a previous report of the water content for the bare silt zone (average of 30%, a whole core of 120 cm) and for the *S. alterniflora* zone (average of 40%, the lower section of 20–120 cm and significantly elevated in the surface 20 cm) in this same coastal wetland (Gao et al., 2012). However, our peak-valley pattern of water content for both cores is different from the aforementioned projects, probably the result of the periodic variation in ground water level that is mainly affected by the tide. The variations in mass magnetic susceptibility for the two cores were quite similar and elevated in the upper layers of the profiles. The magnetic susceptibility is directly linked to the concentration of anthropogenic ferromagnetic particles and dominated by high values of magnetite, which is produced during the combustion of fossil fuel (Kapička et al., 1999). As a result, the pattern of mass magnetic susceptibility enabled us to define the area severely contaminated by industrial activities.

To assess the effects of the sediment properties on the elemental accumulation, the correlation pattern between all of the analytical variables was initially evaluated using a Pearson correlation analysis (Table A1). The water content and dry bulk density have no significant correlations with Ba, Ti, clay, silt and sand but are correlated with other variables. The mass magnetic susceptibility is significantly correlated with Sr, Ti, silt and sand. The clay fraction is significantly correlated with Ti; silt is significantly correlated with Ba and clay; sand is significantly correlated with Ba, Be, Sb, Zn, clay and silt. In general, the mean grain-size is significantly correlated with Al, Ca, Co, Cd, Cs, Fe, K, Li, Mg, Mn, Mo, Na, Pb, ^{210}Pb, Rb, Sb, Tl, V and Zn at the 0.05 or 0.01 level. As a result, the grain size can exert some influence on the distribution of the elements. To eliminate the size effect, the chemical data have been standardized prior to the statistical analyses and normalized to Al to obtain the enrichment factor to understand the in-depth variation.

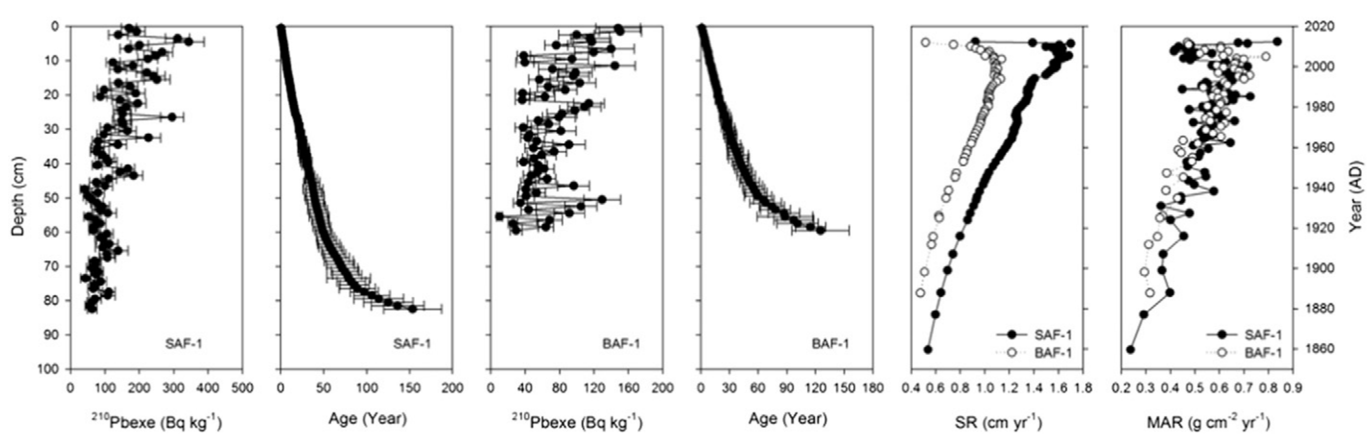

Fig. 3. Radioisotope results of ^{210}Pb activity (Bq kg^{-1}) and chronologies (yr) plotted against depth, and sediment rate (SR, cm yr^{-1}) and mass accumulation rate (MAR, g cm^{-2} yr^{-1}) plotted against ^{210}Pb age (calendar year AD) of the two investigated sediment core samples from the Yancheng coastal wetland in Jiangsu province, China. Error bars represent 1 standard deviation (SD) from counting uncertainty.

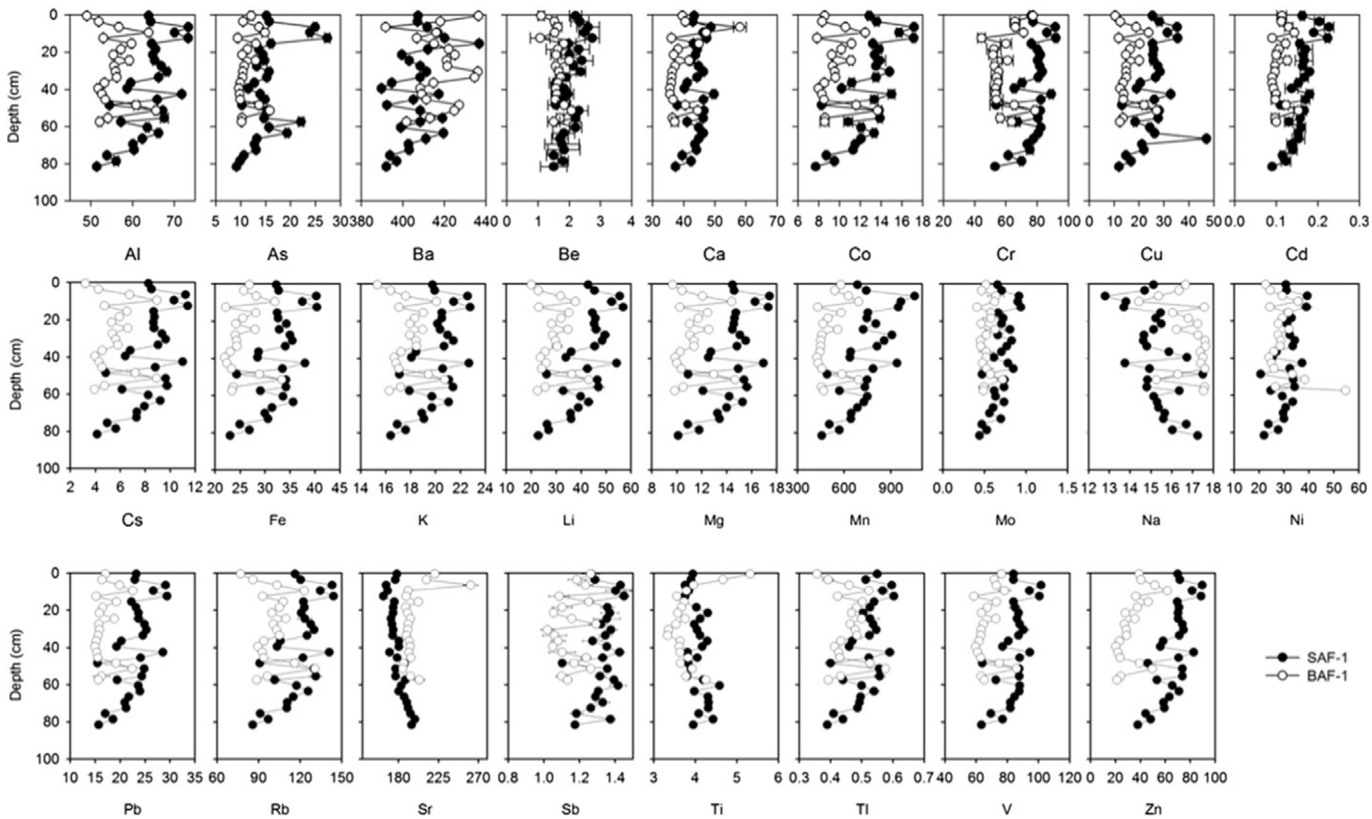

Fig. 4. Concentration variations of major and trace elements of the two investigated sediment core samples from the Yancheng coastal wetland in Jiangsu province, China. Al, Ca, Fe, K, Mg, Na and Ti are expressed as mg g^{-1}, and the other elements are expressed as mg kg^{-1}.

Table 2
Comparison of selected trace metals and metalloids concentrations (mg kg^{-1}, dry weight) of the surface sediment of coastal wetlands in a world context.

Region	As	Cd	Cu	Cr	Ni	Pb	Zn	Data source
Jiangsu province of China								
Yancheng coastal wetland[a]								
Spartina alterniflora flat (SAF-1)	15.2–24.9	0.16–0.23	25.4–35.3	76.3–91.7	30.8–39.3	22.9–29.1	70.0–89.7	This study
Bare flat (BAF-1)	10.5–14.8	0.11–0.14	10.4–23.8	65.8–77.3	22.7–35.7	16.4–22.6	39.0–61.7	This study
Rudong coastal wetland								
Spartina alterniflora flat	6.67	0.084	4.84	44.79	24.32	5.52	72.61	Zhang et al. (2014)
Bare flat	6.49	0.074	3.73	33.55	17.81	4.67	50.86	Zhang et al. (2014)
Linghong tidal flat	12.6–14.5	0.17–1.12	30.4–35.4	68.3–76.6	–[b]	29.9–35.6	70.9–87.4	Liu et al. (2013)
China								
Chongming Dongtan	5.6–9.9	0.19–0.30	23.9–29.7	59.4–62.2	–	17.9–21.9	61.5–71.6	Liu et al. (2013)
Yangtze River (intertidal zone)	–	0.12–0.75	6.9–49.7	36.9–173.0	17.6–48.0	18.3–44.1	47.0–154.0	Zhang et al. (2009)
Coastal Bohai Bay		0.12–0.66	20.1–62.9	60.1–224.5	23.4–52.7	20.9–66.4	55.3–457.3	Gao and Chen (2012)
Jiaozhou Bay	–	0.76	66.5	–	–	28.9	87.2	Dai et al. (2007)
Pearl River Delta	–	1.2–7.8	8.7–140	19.0–59.7	42.1–71.3	48.10–264.2	46.4–533.3	Cheung et al. (2003)
Western Xiamen Bay	–	0.33	44	75	37.4	50	139	Zhang et al. (2007)
Mai Po marshes, Hong Kong	–	6.75	58.4	–	31	–	181	Lau and Chu (2000)
Macao coastal region	12.6–34.6	0.4–8.3	–	4.0–38.6	–	14.5–66.6	–	Ferreira et al. (1996)
Southwestern Taiwan coast	2.8–5.6	0.02–0.25	–	–	–	15.9–29.9	–	Selvaraj et al. (2010)
Northern Beibu Gulf, South China Sea	2.3–13.9	0.02–0.22	–	–	–	–	–	Gan et al. (2013)
Other countries								
Masan Bay, Korea	–	1.24	43.4	67.1	28.8	44.0	206.3	Hyun et al. (2007)
Kranji and Tekong Island, Singapore	–	0.06–0.19	7.7–17.9	40.6–47.3	17.1–26.1	26.1–29.8	49–62	Cuong and Obbard (2006)
Mumbai coast, India	–	–	182.9–190.9	248.1–334.5	95.9–133.4	98.7–133.7	241.6–291.5	Fernandes et al. (2011)
Semarang, Indonesia	–	–	33–72	–	–	18–44	17–36	Takarina et al. (2004)
Peninsular Malaysia	–	–	10.24–119.6	–	–	10.3–125.7	88.7–484.1	Yap and Pang (2011)
Southwest coast of Spain	–	0.79	127.9	59.5	19.9	69.9	323.2	Morillo et al. (2004)
Northern Izmit Bay, Turkey	20–26.8	3.3–8.9	60.6–139	57.9–116.1	38.4–75	23.8–178	500–1190	Pekey et al. (2004)
Soline Bay, Rogoznica, Croatia	–	0.07–0.12	21.1–51.9	–	27.8–40.2	28.5–67.3	17–65	Kljaković-Gašpić et al. (2009)
Bremen Harbor, Germany	–	6	87	131	60	122	790	Hamer and Karius (2002)
Tijuana Estuary, California, USA	–	1.4	26.3	25.4	21.6	36.1	107.1	Weis et al. (2001)

[a] The subsurface 10 cm samples were used to determine the surface data.
[b] Data not available.

3.2. Radioisotope chronology and sediment rate

The radioisotope results for ^{210}Pb were plotted as shown in Fig. 3 for the two cores. Unsupported ^{210}Pb activities (excess ^{210}Pb, $^{210}Pb_{exe}$) present a relatively well-defined logarithmic decrease with depth, and they become negligible at the bottom of both cores because the total ^{210}Pb is in equilibrium with ^{226}Ra (^{214}Pb). The continuous ages were calculated using the CRS dating model and the age-depth models for both cores are plotted (Fig. 3). The sediment records cover approximately 150 years for SAF-1 and 125 years for BAF-1, reaching back to 1860 AD and 1885 AD, respectively. The maximum activities of ^{137}Cs were 1.22 Bq kg^{-1} at the depth of 20 cm for SAF-1 and 1.72 Bq kg^{-1} at the depth of 46 cm for BAF-1, which is consistent with the peak value of ^{137}Cs (1.53 Bq kg^{-1}) in the same wetland (Liu et al., 2010). Because of the low value, ^{137}Cs was detectable with respect to several sections and there is a substantial difference in depth for the maximum ^{137}Cs activities between the two cores. This indicates that the ^{137}Cs technique did not provide a reliable chronostratigraphic index here, which is likely because ^{137}Cs is not well preserved in the silt-fine sand and mud-sand mixed sediments of the Yancheng coastal wetland (Liu et al., 2010). Therefore, the results of the ^{137}Cs activities to check the date are not shown here. Using the ^{210}Pb-derived age, the calculated SR of the SAF-1 core ranged from 0.54 cm yr^{-1} to 1.70 cm yr^{-1} with an average of 1.28 cm yr^{-1}. The BAF-1 core ranged from 0.47 to 1.14 cm yr^{-1} with an average of 0.93 cm yr^{-1}. The MAR of both cores ranged from 0.24 to 0.84 g cm^{-2} yr^{-1} and was averaged as 0.55 g cm^{-2} yr^{-1}. The average SR is approximately consistent with the rate of 1.2 cm yr^{-1} found on the Xingyanggang tidal flat (only 15 km in distance from our study site) (Liu et al., 2010) but smaller than the rate of 3.0 cm yr^{-1} found on the Wanggang salt marsh (approximately 75 km southeast of our study site) (Wang et al., 2005). The overall patterns were quite similar for both cores, with a general increase over time and a maximum value of approximately 2000 AD followed by a decrease in values (Fig. 3). This period of decreasing SR corresponded to the uppermost 5 cm section for both cores, which could possibly be affected by the intensive hydrodynamic force that resulted in less effective deposits.

3.3. Depth variations of major and trace elements in the sediment

The mean, maximum and minimum concentrations of all measured elements of the two investigated sediment core samples from the Yancheng coastal wetland are summarized in Table 1. The ratios of the maximum and minimum values for Al, Ba, Ca, K, Na, Sr and Ti are generally low (<1.5-fold difference), suggesting that the variability of these elements across the profile is small. The corresponding factors for As, Be, Co, Cu, Cd, Cs, Li, Mn, Mo, Ni, Pb and Zn are relatively high (ca. 2-fold difference), suggesting that these elements were probably enriched over the profile. The depth distributions of the major and trace elements are shown in Fig. 4. They are all characterized by an increase in concentration with upward depth, except for Ca, Na, Sr and Ti, which decrease with upward depth. Many studies on heavy metals accumulation in the surface sediments of coastal regions are available across the world for comparisons of their concentrations (Table 2). Firstly, at the local area, the concentrations of As, Cd, Cu, Cr, Ni, Pb and Zn in the surface sediment of the Yancheng coastal wetland are consistent with the corresponding values of the Linghong tidal flat (Liu et al., 2013) ca. 170 km north of our study site; however, our results are slightly higher than the concentrations of elements accumulated in the Rudong coastal wetland (Zhang et al., 2014) ca. 140 km south of our study site. Extended to the national scale or worldwide, the concentrations of those elements in the surface sediments of the Yancheng coastal wetland are at a moderate pollution level.

Most of the elements are significantly correlated at the 0.01 level besides Ba and Ti. Significant correlations are only observed between Ba and Ti, Ti and Cr and Sb and V (Table A1). The statistical evaluation of the distribution dependency of the most correlated elements (except Ba and Ti) in the sediment from different internal or external factors was based on a principal component analysis (PCA) using a varimax rotation solution. Two principle components have initial eigen-values > 1 and explain 86.5% of the total variance in element concentrations in the two cores (Table 3). For most elements at least 67% of their variance can be explained by the exacted components except for ^{210}Pb (45.1%) and Ni (38.7). The first component (PC1) accounts for a large proportion of the variance (45.3%) and is characterized by high positive loadings (0.642–0.888) of As, Cd, Cr, Ca, Fe, Mn, Mo, Pb, ^{210}Pb, Sb, V and Zn and a high negative loading (−0.831) of Na. PC1 clusters the typical pollution elements of As, Cd, Pb, Sb and Zn and probably represent an anthropogenic source. However, this component also consists of typical redox sensitive elements (Fe and Mn); thus, the PC1 may reflect the influence of the depositional process. It is possible that the active elements (Ca and Na) are affected by the post-deposition processes; thus, they are included in this component.

The second component (PC2) accounts for 41.2% of the total variance and is dominated by high positive loadings (0.563–0.831) of Al, Be, Co, Cs, Cu, K, Li, Mg, Ni, Rb and Tl and a high negative loading of Sr (−0.873). PC2 clusters the typical lithogenic elements of Al, K, Rb and Sr and appears to reflect the lithogenic contribution. It is noteworthy that the elements identified in PC1 have moderate loadings associated with PC2, and those identified in PC2 also have moderate loadings associated with PC1. Therefore, the elements could be affected by both sources and depositional process. For example, Zn could also be affected by the lithogenic contribution (27.7%), and 37.9% of Al could be affected by the depositional processes in the coastal wetland environment.

Table 3
Varimax rotated factor matrices for the transformed (Z-scores) elemental concentrations in the two principal components obtained by PCA analysis of the entire Yancheng coastal wetland geochemical dataset (SAF-1 and BAF-1). Significant (>0.5 and <−0.5) factor loadings are designated in bold. Proportion of the total data variance captured by a component is given as Eigenvalue, % Variance and Cumulative variance at the bottom of the table. Percentage of the variance of each element explained by each component and accounted for all the extracted principle components are given in four columns from the right.

	Factor loadings		Partition of communality (%)		Extraction communalities (%)
	PC1	PC2	PC1	PC2	Total
Ca	**0.888**	0.195	78.9	3.8	82.7
Na	**−0.831**	**−0.521**	69.1	27.1	96.2
Cr	**0.812**	0.483	65.9	23.3	89.3
Zn	**0.804**	**0.526**	64.6	27.7	92.3
V	**0.794**	**0.568**	63.0	32.3	95.4
Sb	**0.791**	0.314	62.6	9.9	72.5
Mn	**0.785**	**0.579**	61.6	33.5	95.2
Fe	**0.767**	**0.630**	58.8	39.7	98.4
Cd	**0.767**	**0.594**	58.8	35.3	94.1
Pb	**0.762**	**0.636**	58.1	40.4	98.5
Mo	**0.694**	**0.631**	48.2	39.8	88.0
^{210}Pb	**0.655**	0.146	42.9	2.1	45.1
As	**0.642**	**0.508**	41.2	25.8	67.1
Sr	−0.025	**−0.873**	0.1	76.2	76.3
Tl	0.466	**0.831**	21.7	69.1	90.9
K	**0.536**	**0.824**	28.7	67.9	96.6
Rb	**0.553**	**0.812**	30.6	65.9	96.5
Al	**0.616**	**0.781**	37.9	61.0	98.9
Li	**0.621**	**0.771**	38.6	59.4	98.0
Cs	**0.651**	**0.742**	42.4	55.1	97.4
Be	**0.477**	**0.733**	22.8	53.7	76.6
Co	**0.672**	**0.732**	45.2	53.6	98.7
Mg	**0.674**	**0.730**	45.4	53.3	98.7
Cu	**0.623**	**0.648**	38.8	42.0	80.7
Ni	0.263	**0.563**	6.9	31.7	38.7
Eigen value	11.329	10.298			
% Variance	45.3	41.2			
% Cumulative variance	45.3	86.5			

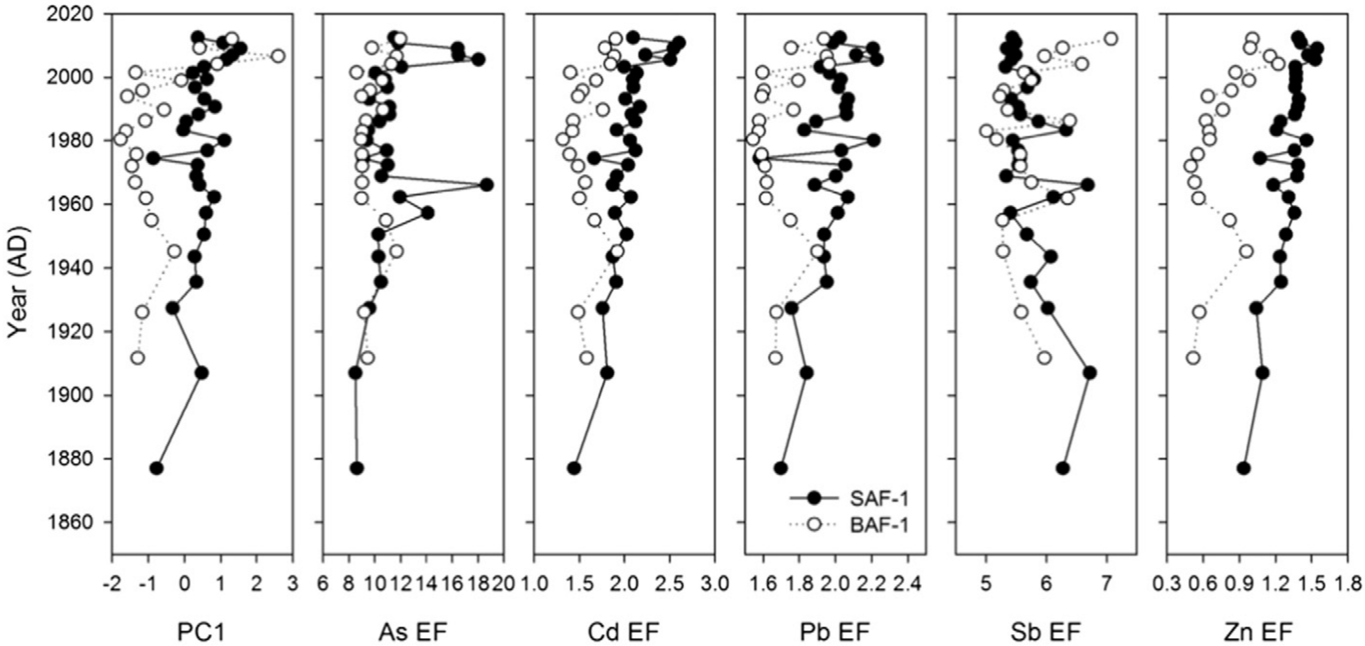

Fig. 5. Temporal variation of the principal component scores (PC1) and enrichment factors (EF, see text for calculation) of As, Cd, Pb, Sb and Zn of the two investigated sediment core samples from the Yancheng coastal wetland in Jiangsu province, China. An EF > 1 indicates that the sample is enriched, relative to the UCC background.

3.4. Historical trends for the pollution elements

The records of factor scores for the pollution component (PC1) are presented in Fig. 5. As stated in Martinez Cortizas et al. (2013), factor scores are non-dimensional, average-centered values which can measure the intensity of each principal component. For the last 20 years, this component of both cores increase with time, indicating an increase in anthropogenic metal pollution in the sediment. Combined with the use of the average metal concentrations of the UCC, the enrichment factors were calculated through normalizing the identified heavy metal content (As, Cd, Pb, Sb and Zn) with respect to a reference metal (i.e., Al) for the two cores (Fig. 5). Given an enrichment factor > 1 suggesting that the sample is enriched relative to background, elevated trends for these pollution elements are observed, especially for As and Sb, corresponding to the sequences of the PC1 scores. As shown by Fig. 5, the two cores present similar patterns with depth for the enrichment factors, still with minor differences due to the different physicochemical properties of the sediment (one is bare flat and the other has plant growth). This is consistent with the grain-size profile characterization which is also affected by the presence of vegetation.

Coastal sediment is usually the result of the mixing of material from various sources, including coastal erosion, biogenic and mineral components, river-borne particles and atmospheric deposits (Abi-Ghanem et al., 2009). Each of these materials has its own natural contributions and is also impregnated by anthropogenic inputs (Callender, 2003). Compared with the multitude of anthropogenic emissions in the environment from the smelting industry, cement production, fossil-fuel combustion, municipal waste incineration, the discharge of sewage

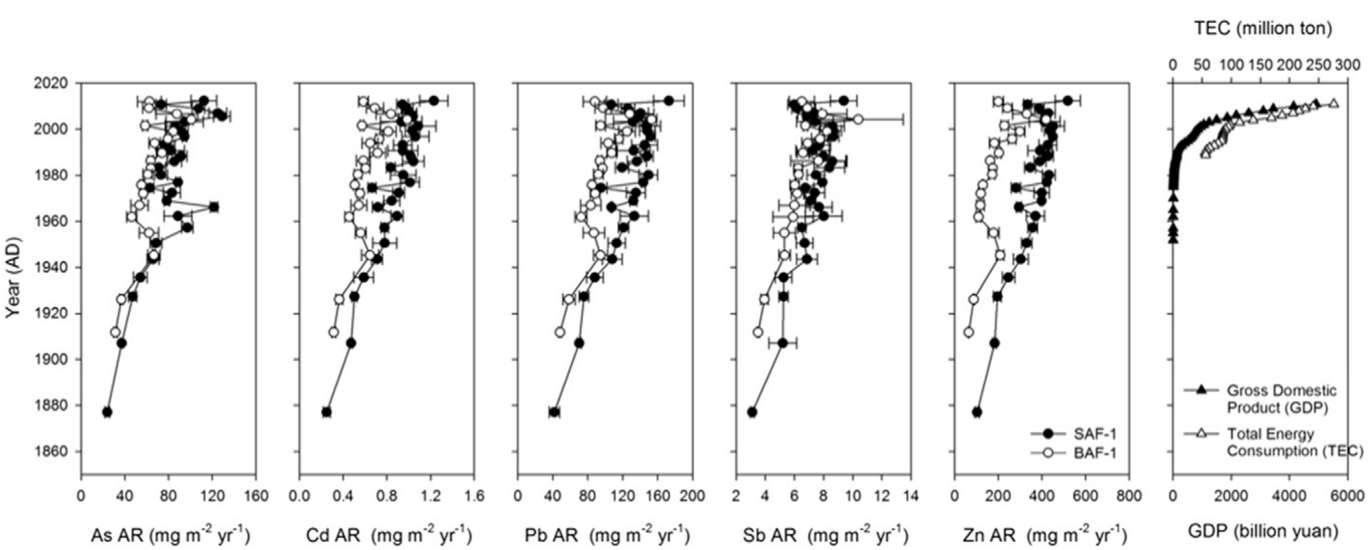

Fig. 6. Temporal variation in accumulation rate (AR, mg m^{-2} yr^{-1}) of the typical pollution elements (As, Cd, Pb, Sb and Zn) identified by the PCA of the two investigated sediment core samples from the Yancheng coastal wetland in Jiangsu province, China. Historical variations of social and economic development indicators in Jiangsu province including gross domestic product (GDP) and total energy consumption (TEC) are also included here for comparison (Jiangsu Provincial Bureau of Statistics, 2013).

sludge, the use of commercial fertilizers and pesticides, and so on, natural inputs may be considered to have very minor effects on the heavy metal accumulation in the sediment in the past, particularly at the Yancheng coast with its extremely rapid pace of recent economic development. Therefore, we did not consider natural changes when we estimated the apparent flux of anthropogenic heavy metals. Assuming the relationship between the sediment accumulation and age derived from ^{210}Pb, we can assign each slice with an estimated age and determine the ARs (mg m^{-2} yr^{-1}) evolution of the typical pollution elements identified by the PCA (Fig. 6). Clearly, there is an increase in the temporal variations of ARs of As, Cd, Pb, Sb and Zn for the Yancheng coastal wetland cores from 1860 through 2013. For the last 20 years especially, the rapid increases in total energy consumption (TEC) and gross domestic product (GDP) in Jiangsu province (Jiangsu Provincial Bureau of Statistics, 2013) corroborate the increase in ARs as well as EFs for those elements (Fig. 6). Therefore, these AR profiles suggest an increase environmental pollution due to anthropogenic activities in the region and more effort is needed to seek a balance between economic development and environmental protection.

4. Conclusions

This study reported a high-resolution geochemical dataset of the physicochemical parameter distribution, ^{210}Pb characteristics and multitrace metal concentrations of two sediment cores collected from the Yancheng coastal wetland in Jiangsu province, China. It has provided important insight to understanding the deposition processes and reconstructing the past pollution history from anthropogenic activities in the area. The grain-size distribution is dominated by silt fine-grain fractions for the coastal wetland sediments and the ^{210}Pb profiles allowed us to date back to 1860 AD for SAF-1 and 1885 AD for BAF-1. The average sediment rate is 1.28 cm yr^{-1} and 0.93 cm yr^{-1} for the two cores, and the mass accumulation rate of both ranges from 0.24 to 0.84 g cm^{-2} yr^{-1} with an average of 0.55 g cm^{-2} yr^{-1}. In total, 26 major and trace elements were measured for the cores, and the accumulation rate, enrichment factor and PCA analyses were used to identify the impact and trends of anthropogenic contributions to the accumulation of pollution elements in the sediments. For the typical pollution elements identified by PCA (As, Cd, Pb, Sb and Zn), their maximum accumulation rates were found near the surface of the sediments, and the increasing accumulation rates for these metals correspond to the increase in economic activity in Jiangsu province over the past 20 years. The enrichment factor values also show a clear anthropogenic signature of heavy metals in the sediments. Heavy metal contamination in a west coastal wetland of the southern Yellow Sea should be considered when developing management strategies for protecting the natural environment and preventing risks and hazards to humans and the ecosystem.

Acknowledgments

We would like to thank Dr. Guixiang Quan (Yancheng Institute of Technology) and Dr. Rong Chen (Nanjing Institute of Geography and Limnology, Chinese Academy of Sciences) for their help in the field. This research was supported by the Natural Science Foundation of Jiangsu Province, China (no. BK20131058), the National Natural Science Foundation of China (no. 41301215), and the National Basic Research Program of China (no. 2012CB956100).

Appendix A. Supplementary data

Supplementary data associated with this article can be found in the online version, at http://dx.doi.org/10.1016/j.gexplo.2015.09.010. These data include Google map of the most important areas described in this article.

References

Abi-Ghanem, C., Chiffoleau, J.F., Bermond, A., Nakhle, K., Khalaf, G., Borschneck, D., Cossa, D., 2009. Lead and its isotopes in the sediment of three sites on the Lebanese coast: identification of contamination sources and mobility. Appl. Geochem. 24, 1990–1999.

Appleby, P.G., 2008. Three decades of dating recent sediments by fallout radionuclides: a review. The Holocene 18, 83–93.

Bai, J., Xiao, R., Cui, B., Zhang, K., Wang, Q., Liu, X., Gao, H., Huang, L., 2011. Assessment of heavy metal pollution in wetland soils from the young and old reclaimed regions in the Pearl River Estuary, South China. Environ. Pollut. 159, 817–824.

Bai, J., Xiao, R., Zhao, Q., Lu, Q., Wang, J., Reddy, K., 2014. Seasonal dynamics of trace elements in tidal salt marsh soils as affected by the flow-sediment regulation regime. PLoS One 9, e107738.

Baldwin, B., Butler, C., 1985. Compaction curves. Am. Assoc. Pet. Geol. Bull. 69, 622–626.

Bao, K., 2015. Coastal wetlands: coupling between ocean and land systems. J. Coast. Res. 31. http://dx.doi.org/10.2112/JCOASTRES-D-14-00190.1.

Bao, K., Xia, W., Lu, X., Wang, G., 2010. Recent atmospheric lead deposition recorded in an ombrotrophic peat bog of Great Hinggan Mountains, Northeast China, from ^{210}Pb and ^{137}Cs dating. J. Environ. Radioact. 101, 773–779.

Bindler, R., Yu, R., Hansson, S., Claben, N., Karlsson, J., 2012. Mining, metallurgy and the historical origin of mercury pollution in lakes and watercourses in Central Sweden. Environ. Sci. Technol. 46, 7984–7991.

Callender, E., 2003. Heavy metals in the environment — historical trends. In: Lollar, B.S., Holland, H.D., Turekian, K.K. (Eds.), Environmental GeochemistryTreatise on Geochemistry 9. Elsevier, Oxford, pp. 67–106.

Cheung, K., Poon, B., Lan, C., Wong, M., 2003. Assessment of metal and nutrient concentrations in river water and sediment collected from the cities in the Pearl River Delta, South China. Chemosphere 52, 1431–1440.

Chuai, X., Huang, X., Wang, W., Wu, C., Zhao, R., 2014. Spatial simulation of land use based on terrestrial ecosystem carbon storage in coastal Jiangsu China. Sci. Rep. 4.

Cuong, D.T., Obbard, J.P., 2006. Metal speciation in coastal marine sediments from Singapore using a modified BCR-sequential extraction procedure. Appl. Geochem. 21, 1335–1346.

Dai, J., Song, J., Li, X., Yuan, H., Li, N., Zheng, G., 2007. Environmental changes reflected by sedimentary geochemistry in recent hundred years of Jiaozhou Bay, North China. Environ. Pollut. 145, 656–667.

Fang, S.B., Xu, C., Jia, X.B., Wang, B.Z., An, S.Q., 2010. Using heavy metals to detect the human disturbances spatial scale on Chinese Yellow Sea coasts with an integrated analysis. J. Hazard. Mater. 184, 375–385.

Fernandes, L., Nayak, G.N., Ilangovan, D., Borole, D.V., 2011. Accumulation of sediment, organic matter and trace metals with space and time, in a creek along Mumbai coast, India. Estuar. Coast. Shelf Sci. 91, 388–399.

Ferreira, M.F., Chiu, W., Cheok, H., Cheang, F., Sun, W., 1996. Accumulation of nutrients and heavy metals in surface sediments near Macao. Mar. Pollut. Bull. 32, 420–425.

Gan, H., Lin, J., Liang, K., Xia, Z., 2013. Selected trace metals (As, Cd and Hg) distribution and contamination in the coastal wetland sediment of the northern Beibu Gulf, South China Sea. Mar. Pollut. Bull. 66, 252–258.

Gao, X., Chen, C.T.A., 2012. Heavy metal pollution status in surface sediments of the coastal Bohai Bay. Water Res. 46, 1901–1911.

Gao, J., Bai, F., Yang, Y., Gao, S., Liu, Z., Li, J., 2012. Influence of *Spartina* colonization on the supply and accumulation of organic carbon in tidal salt marshes of northern Jiangsu province, China. J. Coast. Res. 28, 486–498.

Gao, C., Bao, K., Lin, Q., Zhao, H., Zhang, Z., Xing, W., Lu, X., Wang, G., 2014a. Characterizing trace and major elemental distribution in late Holocene in Sanjiang Plain, Northeast China: paleoenvironmental implications. Quat. Int. 349, 376–383.

Gao, S., Du, Y., Xie, W., Gao, W., Wang, D., Wu, X., 2014b. Environment–ecosystem dynamic processes of *Spartina alterniflora* salt-marshes along the eastern China coastlines. Sci. China Earth Sci. 57, 2567–2586.

Hamer, K., Karius, V., 2002. Brick production with dredged harbour sediments. An industrial-scale experiment. Waste Manag. 22, 521–530.

Hong, S.M., Candelone, J.P., Patterson, C.C., Boutron, C.F., 1994. Greenland ice evidence of hemispheric lead pollution two millennia ago by Greek and Roman civilizations. Science 265, 1841–1843.

Hyun, S., Lee, C., Lee, T., Choi, J., 2007. Anthropogenic contributions to heavy metal distributions in the surface sediments of Masan Bay, Korea. Mar. Pollut. Bull. 54, 1059–1068.

Jamshidi-Zanjani, A., Saeedi, M., 2013. Metal pollution assessment and multivariate analysis in sediment of Anzali international wetland. Environ. Earth Sci. 70, 1791–1808.

Jayaprakash, M., Urban, B., Velmurugan, P., Srinivasalu, S., 2010. Accumulation of total trace metals due to rapid urbanization in microtidal zone of Pallikaranai marsh, South of Chennai, India. Environ. Monit. Assess. 170, 609–629.

Jiangsu Provincial Bureau of Statistics, 2013. Jiangsu Statistical Yearbook. China Statistics Press.

Kapička, A., Petrovský, E., Ustjak, S., Macháčková, K., 1999. Proxy mapping of fly-ash pollution of soils around a coal-burning power plant: a case study in the Czech Republic. J. Geochem. Explor. 66, 291–297.

Ke, C., Zhang, D., Wang, F., Chen, S., Schmullius, C., Boerner, W., Wang, H., 2011. Analyzing coastal wetland change in the Yancheng National Nature Reserve, China. Reg. Environ. Chang. 11, 161–173.

Kirwan, M.L., Megonigal, J.P., 2013. Tidal wetland stability in the face of human impacts and sea-level rise. Nature 504, 53–60.

Kljaković-Gašpić, Z., Bogner, D., Ujević, I., 2009. Trace metals (Cd, Pb, Cu, Zn and Ni) in sediment of the submarine pit Dragon ear (Soline Bay, Rogoznica, Croatia). Environ. Geol. 58, 751–760.

Lau, S., Chu, L., 2000. The significance of sediment contamination in a coastal wetland, Hong Kong, China. Water Res. 34, 379–386.

Le Roux, G., Weiss, D., Grattan, J., Givelet, N., Krachler, M., Cheburkin, A., Rausch, N., Kober, B., Shotyk, W., 2004. Identifying the sources and timing of ancient and medieval atmospheric lead pollution in England using a peat profile from Lindow bog, Manchester. J. Environ. Monit. 6, 502–510.

Leorri, E., Cearreta, A., García-Artola, A., Irabien, M.J., Blake, W.H., 2013. Relative sea-level rise in the Basque coast (N Spain): different environmental consequences on the coastal area. Ocean Coast. Manag. 77, 3–13.

Li, J., Gao, S., 2013. Estimating deposition rates using a morphological proxy of *Spartina alterniflora* plants. J. Coast. Res. 29, 1452–1463.

Liu, Z., Pan, S., Liu, X., Gao, J., 2010. Distribution of Cs-137 and Pb-210 in sediments of tidal flats in north Jiangsu Province. J. Geogr. Sci. 20, 91–108 (in Chinese with English abstract).

Liu, Z., Pan, S., Yin, Y., Ma, R., Gao, J., Xia, F., Yang, X., 2013. Reconstruction of the historical deposition environment from ^{210}Pb and ^{137}Cs records at two tidal flats in China. Ecol. Eng. 61, 303–315.

Mahiques, M.M., Figueira, R.C.L., Salaroli, A.B., Alves, D.P.V., Gonçalves, C., 2013. 150 years of anthropogenic metal input in a biosphere reserve: the case study of the Cananéia–Iguape coastal system, southeastern Brazil. Environ. Earth Sci. 68, 1073–1087.

Martinez Cortizas, A., Lopez-Merino, L., Bindler, R., Mighall, T., Kylander, M., 2013. Atmospheric Pb pollution in N Iberia during the late Iron Age/Roman times reconstructed using the high-resolution record of La Molina mire (Asturias, Spain). J. Paleolimnol. 50, 71–86.

Monteiro, F.F., Cordeiro, R., Santelli, R., Machado, W., Evangelista, H., Villar, L., Viana, L.C., Bidone, E., 2012. Sedimentary geochemical record of historical anthropogenic activities affecting Guanabara Bay (Brazil) environmental quality. Environ. Earth Sci. 65, 1661–1669.

Morillo, J., Usero, J., Gracia, I., 2004. Heavy metal distribution in marine sediments from the southwest coast of Spain. Chemosphere 55, 431–442.

Nriagu, J.O., 1996. A history of global metal pollution. Science 272, 223–224.

Pacyna, J.M., Pacyna, E.G., 2001. An assessment of global and regional emissions of trace metals to the atmosphere from anthropogenic sources worldwide. Environ. Rev. 9, 269–298.

Pekey, H., Karakaş, D., Ayberk, S., Tolun, L., Bakoğlu, M., 2004. Ecological risk assessment using trace elements from surface sediments of İzmit Bay (Northeastern Marmara Sea) Turkey. Mar. Pollut. Bull. 48, 946–953.

Pennings, S.C., 2012. Ecology: the big picture of marsh loss. Nature 490, 352–353.

Perillo, G., Wolanski, E., Cahoon, D., Brinson, M., 2009. Coastal Wetlands: An Integrated Ecosystem Approach. Elsevier, Amsterdam, The Netherlands, p. 974.

Qiu, J., 2011. China faces up to 'terrible' state of its ecosystems. Nature 471, 19-19.

Regnier, P., et al., 2013. Anthropogenic perturbation of the carbon fluxes from land to ocean. Nat. Geosci. 6, 597–607.

Reimann, C., de Caritat, P., 2005. Distinguishing between natural and anthropogenic sources for elements in the environment: regional geochemical surveys versus enrichment factors. Sci. Total Environ. 337, 91–107.

Rydberg, J., Martinez Cortizas, A., 2014. Geochemical assessment of an annually laminated lake sediment record from northern Sweden: a multi-core, multi-element approach. J. Paleolimnol. 51, 499–514.

Selvaraj, K., Parthiban, G., Chen, C.T.A., Lou, J.Y., 2010. Anthropogenic effects on sediment quality offshore southwestern Taiwan: assessing the sediment core geochemical record. Cont. Shelf Res. 30, 1200–1210.

Takarina, N., Browne, D., Risk, M., 2004. Speciation of heavy metals in coastal sediments of Semarang, Indonesia. Mar. Pollut. Bull. 49, 854–874.

UNECE, 1994. United Nations Economic Commission for Europe, Heavy metals emissions, Task Force on Heavy Metals Emissions State-of-the-Art Report. The Czech Republic, Prague.

Wang, A., Gao, S., Jia, J., Pan, S., 2005. Contemporary sedimentation rates on salt marshes at Wanggang, Jiangsu, China. Acta Geograph. Sin. 60, 61–70 (in Chinese with English abstract).

Weis, D.A., Callaway, J.C., Gersberg, R.M., 2001. Vertical accretion rates and heavy metal chronologies in wetland sediments of the Tijuana Estuary. Estuaries 24, 840–850.

Yap, C., Pang, B., 2011. Assessment of Cu, Pb, and Zn contamination in sediment of north western Peninsular Malaysia by using sediment quality values and different geochemical indices. Environ. Monit. Assess. 183, 23–39.

Zhang, L., Ye, X., Feng, H., Jing, Y., Ouyang, T., Yu, X., Liang, R., Gao, C., Chen, W., 2007. Heavy metal contamination in western Xiamen Bay sediments and its vicinity, China. Mar. Pollut. Bull. 54, 974–982.

Zhang, W., Feng, H., Chang, J., Qu, J., Xie, H., Yu, L., 2009. Heavy metal contamination in surface sediments of Yangtze River intertidal zone: an assessment from different indexes. Environ. Pollut. 157, 1533–1543.

Zhang, L., Du, Y., Wang, D., Gao, S., Gao, W., 2014. Distribution patterns and pollution assessments of heavy metals in the *Spartina alterniflora* salt-marsh wetland of Rudong, Jiangsu province. Environ. Sci. 35, 2401–2410 (in Chinese with English abstract).